THE JOURNAL OF PHYSICAL CHEMISTRY C

Article

pubs.acs.org/JPCC

Nanostructured Few-Layer Graphene with Superior Optical Limiting Properties Fabricated by a Catalytic Steam Etching Process

Zhenyu Sun,[†] Ningning Dong,[‡] Kunpeng Xie,[†] Wei Xia,[†] Dennis König,[§] Tharamani Chikka Nagaiah,[∥] Miguel D. Sánchez,[†,⊥] Petra Ebbinghaus,[#] Andreas Erbe,[#] Xiaoyan Zhang,[‡] Alfred Ludwig,[§] Wolfgang Schuhmann,[∥] Jun Wang,*[,‡] and Martin Muhler*[,†]

[†]Laboratory of Industrial Chemistry, Ruhr-University Bochum, D-44780, Bochum, Germany

[‡]Key Laboratory of Materials for High-Power Laser, Shanghai Institute of Optics and Fine Mechanics, Chinese Academy of Sciences, Shanghai 201800, China

[§]Department of Mechanical Engineering, Institute for Materials, Ruhr-University Bochum, D-44780, Bochum, Germany

[∥]Analytische Chemie-Elektroanalytik & Sensorik, Ruhr-University Bochum, D-44780, Bochum, Germany

[⊥]Departamento de Física and Instituto de Física del Sur, Universidad Nacional del Sur- CONICET, 8000, Bahía Blanca, Argentina

[#]Max-Planck-Institut für Eisenforschung GmbH, Max-Planck-Str. 1, 40237, Düsseldorf, Germany

Supporting Information

ABSTRACT: Tailoring the morphology and structure of graphene can result in novel properties for advanced applications. Here, we demonstrate the fabrication of nanostructured few-layer graphene through a mild etching process via catalytic steam gasification of carbon by Fe nanoparticles (NPs). Controlling the reaction temperature, steam concentration, and the loading density of the NPs enables the fine-tuning of the etching level of graphene. Well-defined nanotrenches with a width of less than 25 nm were formed by channeling of the catalytic NPs. Etching caves and quasi-semicircular etched edges were observed as well. The nonlinear optical properties of the resulting nanostructured graphene were studied under a 532 nm nanosecond pulse laser through an open-aperture apparatus. At the same level of the linear extinction coefficient, it exhibits superior optical limiting performance in comparison with pristine graphene and C_{60}, showing a large potential in nanophotonic devices. This enhancement is ascribed to the defects formed by etching resulting in a finite band gap in nanostructured graphene.

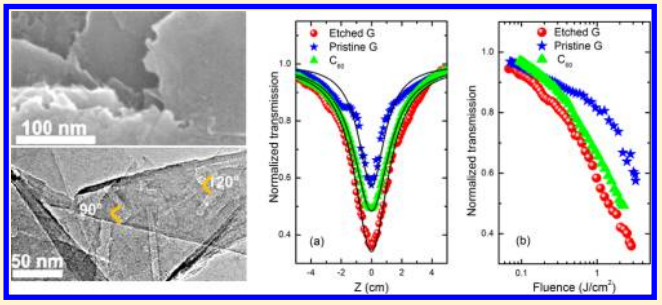

INTRODUCTION

Pristine graphene, a monatomic sheet of honeycomb sp^2 hybridized carbon atoms, is a semimetal with zero bandgap, which leads to poor switching behavior in transistors and thus imposes limits in technologically significant applications such as nanoelectronics and nanophotonic devices.[1] An effective strategy for addressing this issue is to modulate the size, geometry, and edge crystallinity of graphene that enables the tailoring of its band structure.[2] While nanostructured graphene and graphite were achieved using hydrogen plasma etching,[3] electron beam lithography,[4] scanning tunneling microscopy lithography,[5] and atomic force microscopy anodic oxidation,[6] producing graphene with well-defined crystallographic edges remains an ongoing challenge. It should also be noted that etching of graphene was usually carried out first by fixing graphene onto a substrate, and consequently, large-scale production of tailored graphene with these protocols is unrealistic. Despite interesting reports on the electronic transport properties of etched graphene structures,[3] further insights into their nonlinear optical (NLO) and optical limiting (OL) properties are lacking.

Graphene-based materials show great promise in ultrafast lasers as saturable absorbers due to their ultrafast carrier relaxation times and broadband NLO responses to nanosecond pulses from the visible to the near-infrared regime, in contrast to C_{60}, the benchmark material, that only has a limiting NLO response in the visible spectral region.[7−9] The unique two-dimensional sp^2 carbon network of graphene also permits formation of versatile NLO hybrid structures by attaching functional materials, such as CdS quantum dots.[10] Recent results demonstrated that there exist structure-to-NLO relationships of graphene samples.[11,12] It was found that the optical transmittance and limiting properties of graphene were sensitive to oxygen-containing functional groups, flake size, and structural defects. Thus, chemical doping and functional-

Received: February 19, 2013
Revised: April 30, 2013
Published: May 14, 2013

   dx.doi.org/10.1021/jp401736n | J. Phys. Chem. C 2013, 117, 11811−11817

ization are suitable routes to tune graphene materials for optical applications. These scenarios warrant further exploration of the NLO performance of nanostructured graphene with varying morphologies.

Here, we present a novel technique for the controlled etching of few-layer graphene via catalytic steam gasification of carbon by Fe nanoparticles (NPs). The process has a number of advantages. First, few-layer graphene obtained by exfoliation of natural graphite in isopropanol (*i*-PrOH) was used as the starting material. This allows for uniform deposition of catalytic NPs on graphene on the basis of solution chemistry[13] and therefore high yields of etched graphene after the steam gasification. In addition, the low boiling point of *i*-PrOH permits its easy removal from the graphene surface before etching. In this way, the influence from the adsorbed solvent that can act as carbon sources and saturate the Fe NPs during the etching process is ruled out. Second, the size of the catalytic NPs is small with a mean particle size of about 10.9 nm derived from analyzing 30 different NPs by transmission electron micrcoscopy (TEM) but uniform with a standard size deviation of 1.8 nm enabling nanocutting of graphene. Third, in contrast to the strong oxidation of graphene in oxygen, steam gasification of graphene is milder and slower, thus allowing for better control over the etching progress. The etching is presumed to occur selectively at the interface between graphene and the Fe NPs. Only water and iron, which are readily available, are employed in this eco-friendly process, producing H_2 and CO as major components of synthesis gas.[14] The degree of etching can be conveniently tailored by tuning the reaction temperature, steam concentration, as well as the loading level of the Fe NPs. More importantly, we demonstrate for the first time that catalytically etched graphene shows superior nonlinear optical response in comparison with pristine graphene and C_{60}.

EXPERIMENTAL SECTION

Materials. All chemicals used in this work were of analytical grade and used as supplied. Isopropanol (*i*-PrOH, product number 20842.312) was supplied by VWR International. Graphite powder was provided by Sigma-Aldrich (product number 332461) and used without further treatments. $Fe(NO_3)_3{\cdot}9H_2O$ was obtained from Sigma-Aldrich (product number 216828).

Preparation of Graphene Dispersions in *i*-PrOH. Graphene dispersions were prepared by adding graphite at an initial graphite concentration of 5 mg mL^{-1} to 400 mL of *i*-PrOH in 500 mL capped round-bottom flasks. Ultrasonication was carried out in a sonic bath (Bandelin Sonorex, 100 W, 35 kHz). To maintain sonication efficiency and prevent overheating, the flask was kept in an ice-water bath. After being subjected to 64 h of sonication, the samples were left to stand overnight to allow any unstable graphite aggregates to form and then centrifuged at 1000 rpm for 30 min. After centrifugation, the top two-thirds of the dispersion was gently extracted by pipetting. The graphene concentration (C_G) was determined by measuring the mass of the remaining solid per volume of the dispersion after removal of the solvent by evaporation. The dispersion was then diluted to 0.05 mg mL^{-1} for further use.

Deposition of Iron Oxide NPs on Graphene. Typically, 20 mL of a graphene dispersion (C_G = 0.05 mg mL^{-1}) in *i*-PrOH was first subjected to 2 min tip sonication (Bandelin Sonoplus HD 3100, 100 W, 20 kHz, 3 mm diameter tip). Subsequently, 1 mL of $Fe(NO_3)_3{\cdot}9H_2O$ and 1 mL of NaOH, both dissolved in a mixing solvent (90 vol % of the low-boiling point solvent and 10 vol % of distilled water), in turn were added dropwise into the dispersion under tip sonication within 2 min in each case. The molar concentration of NaOH was 3 times higher than that of the precursor. All synthetic processes were conducted at room temperature. Very small iron hydroxide NPs with size of ∼2 nm were uniformly deposited onto graphene resulting from the reaction between $Fe(NO_3)_3{\cdot}9H_2O$ and NaOH facilitated by a high-intensity ultrasound. The system was ultracentrifuged, and the collected precipitate was washed thoroughly with distilled water and then vacuum-dried at 60 °C for 6 h. The obtained sample was calcined in synthetic air (20 vol % O_2 in N_2) at 300 °C for 10 min before etching.

Etching of Graphene. In a typical etching experiment, the iron oxide-loaded graphene was reduced and annealed in H_2 and Ar (1:9, 150 mL min^{-1}) with a heating rate of 7.5 °C min^{-1} up to the reaction temperature (such as 650 °C). H_2 (15 mL min^{-1}), Ar (134.7 mL min^{-1}), and H_2O vapor (0.3 mL min^{-1}) were then introduced to the reactor at a total flow rate of 150 mL min^{-1}. The water vapor was introduced by flowing Ar through a saturator filled with a mixture of ice and water. Gas-phase CO originating from the steam gasification was monitored online using a gas detector. After etching for 30 min, the reactor was cooled to room temperature. Finally, the resultant sample was acid treated (1 M HCl) under stirring at ambient temperature for 24 h and then filtered and washed with distilled water followed by drying for further characterization.

Characterization. UV−vis absorption spectra of pristine and etched graphene dispersions in *i*-PrOH were conducted using a Varian Cary 60 spectrophotometer. X-ray diffraction (XRD) was performed with a D/MAX−RC diffractometer operated at 30 kV and 100 mA with Cu Kα radiation.

X-ray photoelectron spectroscopy (XPS) measurements were carried out in an ultra-high vacuum (UHV) setup equipped with a monochromatic Al Kα X-ray source ($h\nu$ = 1486.6 eV), operated at 14.5 kV and 35 mA, and a high-resolution Gammadata−Scienta SES 2002 analyzer. The base pressure in the measurement chamber was maintained at about 2×10^{-9} mbar. The resolution spectra were carried out in the fixed transmission mode with pass energy of 200 eV, resulting in an overall energy resolution of 0.25 eV. A flood gun was applied to compensate the charging effects. The binding energy scales were re-calibrated based on the C 1s peak of low-defect pure graphite at 284.6 eV. The Casa XPS software with a Gaussian−Lorentzian product function and Shirley background subtraction was used for peak deconvolution. All spectra were normalized to the corresponding C 1s region area for better comparison.

Scanning electron microscopy (SEM) was carried out using a field emission microscope (FEI Quanta 600 FEG) operated at 20 kV and equipped with an energy-dispersive X-ray spectrometer (EDX). Transmission electron microscopy (TEM) and high-resolution TEM images were recorded with a transmission electron microscope (FEI Tecnai F20) operated at 200 kV. TEM specimens were prepared by pipetting a few milliliters of the dispersions of pristine or etched graphene in *i*-PrOH onto holey carbon mesh grids (400 mesh).

Atomic force microscopy (AFM) measurements were performed in tapping mode with a Nanowizard 3 AFM controlled by a JPK SPM control station III. Cantilevers were made of doped single crystal Si (NCS 15, 325 kHz resonance)

dx.doi.org/10.1021/jp401736n | J. Phys. Chem. C 2013, 117, 11811−11817

with a tip (radius <10 nm, force constant ≈ 46 N m^{-1}). Samples for AFM were prepared by drop casting the dispersions of pristine or etched graphene in *i*-PrOH onto a freshly cleaved mica wafer and dried at an ambient environment.

Raman spectra of graphene films and graphite powder were attained with a Horiba Jobin Yvon LabRam 2 confocal Raman microscope with a HeNe Laser excitation at 633 nm (1.96 eV) with a power of 3.5 mW. Deposited thin films were prepared by vacuum filtration of dispersions of pristine or etched graphene in *i*-PrOH onto porous nylon membranes (Whatman, 0.2 μm pore size, 47 mm membrane diameter) and dried at room temperature. Measurements were taken with 5 s of exposure time using a long working distance objective of 50-fold magnification and aperture of 0.5 yielding a beam diameter of ~600 nm in the focus. The peak maximum intensity ratio M_D/M_G was obtained by taking the peak intensities following baseline corrections to remove residual fluorescence. Peak area ratios A_D/A_G were obtained by a subsequent fit of the D and G bands to Gaussian peaks.

Optical Limiting Measurements. To test the NLO response, pristine and etched graphene were both dispersed in dimethylformamide (DMF), and C_{60} was dispersed in toluene. For the comparison of the NLO properties, the concentrations were adjusted to ensure that the three suspensions had the same linear transmission of approximately 50% with OD = 0.3. A standard open-aperture Z-scan apparatus was used to measure the NLO properties of graphene dispersions. The total transmittance through the sample is measured as a function of incident laser intensity when the sample is gradually moved through the focus point of a lens (along the *z*-axis). The optical arrangement is identical to what we used in our previous work.[8] All experiments were performed using 6 ns pulses from a Q-switched Nd:YAG laser. The beam was tightly focused with a lens with 20 cm focal length. The laser was operated at the second harmonic, 532 nm, with a pulse repetition rate of 10 Hz. All samples were tested in 0.1 cm quartz cells.

RESULTS AND DISCUSSION

Figure 1 shows typical TEM images of pristine graphene (Figure 1a) and iron oxide NP-decorated graphene before (Figure 1b) and after etching (Figure 1c–e). Interestingly, hollow NPs of size ~15 nm were obtained after steaming at 650 °C for 30 min. The core of the NPs has a diameter of ~5.5 nm, and the shell is ~3.7 nm thick. The evolution of the hollow structure can be due to the nanoscale Kirkendall Effect.[15] To be specific, upon introducing steam, the outer surface of the NPs is oxidized forming an oxide layer. At extended reaction periods, the outward diffusion of Fe through the oxide layer proceeds more rapidly than the inward diffusion of H_2O. The Fe core was thus gradually consumed and shrank leading to the formation of a core–shell–void intermediate structure.

After removal of the NPs by washing with dilute hydrochloric acid, etching caves and trenches were clearly seen by SEM that were heterogeneously distributed on the surface of graphene (Figure 2a,b). This is in sharp contrast to the continuous and smooth surface of the starting graphene (Figure 1a and Supporting Information Figure S1a). An alternate quasi-semicircular shape was commonly observed at etched edges, roughly as a fingerprint of the catalyst particle. The diameter of the semicircle appears to be dependent on the size of the NPs. When the NPs become deactivated by poisoning probably due

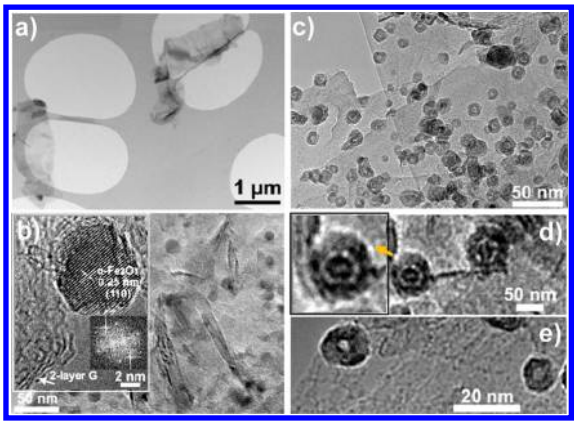

Figure 1. TEM images of (a) pristine graphene, (b) graphene decorated with iron oxide NPs prior to and (c) after steaming (650 °C, 0.3 mL min^{-1} H_2O vapor), (d) iron oxide NPs with a bridge linking the core and the shell, and (e) hollow iron oxide NPs. Inset in (b): HRTEM image and fast Fourier transform (FFT) of the NP showing its single crystalline nature. Inset in (d): A close-up of the NP displayed in d.

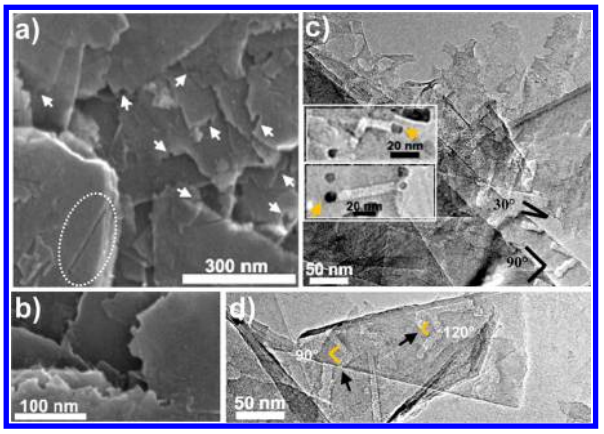

Figure 2. (a) Low- and (b) high-magnification SEM images of graphene after steaming (650 °C, 0.3 mL min^{-1} H_2O vapor). TEM images of etched graphene (c) with semicircular edges and trenches deflecting from the edges at angles of 30 and 90° and (d) with trenches reflecting away from previous parts at angles of 90 and 120°. The insets in (c) show that iron oxide NPs position at the end of trench tracks.

to coke deposition, the etched regimes reconstruct dynamically but unlikely grow further in size. Close inspection by TEM reveals that most etched tracks commence from the graphene edges, which may be due to two reasons. First, the deposition of NPs on the edges with dangling bonds is energetically favorable. On the other hand, activation barriers for attack at defective edges are lower compared to an attack on the hexagonal basal plane.[16] Aside from the semicircular geometric structure, well-defined nanotrenches were observed as well (Figure 2c,d). The majority of these trenches is smooth with a width of less than 25 nm. The trenches run along straight lines and intermittently deflect from their path or reflect away from previously etched parts at angles of 30, 90, and 120° along a specific crystallographic orientation. TEM micrographs in the insets of Figure 2c show that the NPs are positioned at the end of the trench tracks and remain attached to the graphene interface albeit of no support beneath, indicating that the trenches are formed by channeling of the catalytic NPs. Larger NPs seem to channel longer trenches probably due to their

dx.doi.org/10.1021/jp401736n | J. Phys. Chem. C 2013, 117, 11811–11817

higher surface areas and lower tendency to deactivate relative to smaller NPs. This assumption is to some extent supported by TEM observations (Figure S3, Supporting Information). Channeling NPs tend to turn away when approaching an existing trench, presumably due to Coulomb interactions between the Fe NPs and the enhanced electronic density of states at the etched edge.[17] Hence, intersection of trenches rarely occurred. Such a scenario may allow designing of connected graphene nanostructures.

High-resolution TEM (HRTEM) observations illustrate that etching is prone to occur on thin sheets (≤5 layers), probably arising from their larger deformation and richer sp^3 domains relative to thick ones (>5 layers) (Figure 3a,b). The roughness

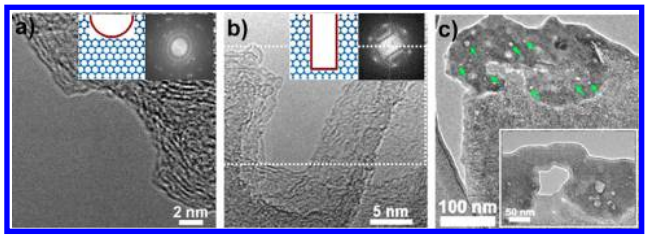

Figure 3. Drawing and HRTEM images of the edges of graphene with a (a) semicircular and (b) rectangular shape after etching (650 °C, 0.3 mL min^{-1} H_2O vapor). (c) TEM image of an etched flake, showing a porous structure. The diffraction pattern (top right inset in a) clearly shows (1100) and (2110) spots. The more intense feature of (2110) spots confirms that this is a few-layer graphene. The top right inset in (b) depicts a FFT of the region enclosed by the white dashed square. The (1100) spots can be seen, while the (2110) spots are too weak to see indicative of monolayer graphene. Inset in (c): An enlarged view of etched flakes.

of the etched edges is estimated to be ∼1 nm by HRTEM, only 7 times of the C−C distance (a_{c-c} = 0.142 nm). Etch pits were also observed in the defective regions of the basal plane, as shown in Figure 3c. Atomic force microscopy (AFM) analysis observed an etched flake with a thickness of about 0.6 nm consistent with monolayer graphene (Figure 4a,b). In Figure

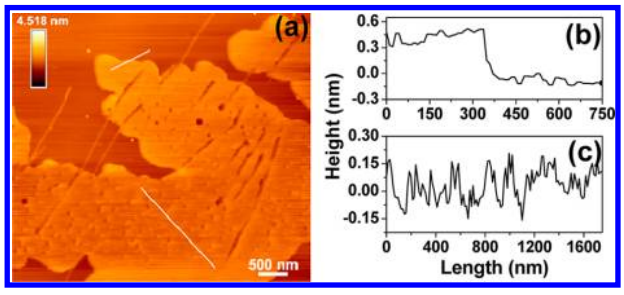

Figure 4. (a) AFM image of graphene sheets. Pores and cuts can be clearly seen after etching. Height profiles along the top (b) and bottom (c) white lines in (a).

4c, the rugged topographic height profiles may result from the etch holes/trenches distributed on the flake. Note that the length of the trenches is up to 2.3 μm, whereby the channeling speed is as high as ∼77 nm per minute considering the etching time of 30 min.

The UV−vis spectrum of graphene after etching exhibits similar absorption features as untreated graphene (Figure S4, Supporting Information). The strong peak at about 265 nm (4.7 eV) arises from the π-plasmon resonance that is commonly observed in graphitic materials, whereas the spectra are featureless up to the visible range (800 nm) with a steady decrease in absorbance with increasing wavelength. Shown in Figure 5a are XRD patterns of the starting graphite, pristine and etched graphene. The diffraction peaks at 26.6 and 54.2° in traces A, B, and C in Figure 5a originate from the (002) and (004) reflections of the graphitic structure, respectively. The two peaks in trace A are almost at the same positions as those in traces B and C, suggesting that the graphite lattice parameters were restored after exfoliation and even etching. However, in traces B and C, weakening in the relative intensity of the (004) peak occurred, and no (006) reflection was observed. This concurs with those observed for sublattices consisting of fewer than four graphene layers.[18] A broad peak at 43.5° appeared, corresponding to the (100) plane of graphene, whereas no peak characteristic of graphene oxide at 10° was found. A remarkable broadening of the (002) peak, as shown in trace C, was clearly observed. The full width at half-maximum (fwhm) of the peak was 1.57° as opposed to that of 0.50° for both graphite and pristine graphene. It may correlate with the small and nonuniform grain sizes of etched graphene.[18] We also found that the relative intensity of the (100) peak increased after etching.

X-ray photoelectron spectroscopy (XPS) analysis (see Supporting Information, Figure S5) showed that the atomic concentration of oxygen was as low as 1.6% after steaming. This value compares favorably with that of 2% for graphite and of 3.2% for graphene before etching, suggesting that etched graphene has undergone deoxygenation. We studied the plasmon satellites occurring at approximately 5.6 and 7.2 eV above the main line of carbon (Figure S5b, Supporting Information). These structures are closely associated with the $\pi-\pi^*$ and $2p-\pi$ interactions and also interfere with O-containing functional groups. A decrease in intensity was observed for graphene even after etching, which was further confirmed by subtracting the spectrum from that of graphite (Figure 5b). The depletion in the region suggests a loss in graphite stacking consistent with the random orientation of graphene sheets. Additionally, broadening of the peak with binding energy lower than that of the C−C occurred after steaming, which is related to the generation of more defects induced by the catalytic etching.

Figure 5c presents representative Raman spectra of the original graphite powder and thin films formed by vacuum filtration of the graphene dispersions in *i*-PrOH before and after etching. The Raman spectra of pristine and etched graphene both display three prominent peaks: a G band at about 1572 cm^{-1}, a second-order two-phonon mode 2D band at about 2642 cm^{-1}, and a disorder-related D peak at about 1325 cm^{-1}.[13] The G band is typically assigned to the first-order scattering of the E_{2g} mode of C sp^2 atoms, while the D band is associated with the breathing mode of κ-point phonons of A_{1g} symmetry. An additional weak D′ peak (∼1616 cm^{-1}) appeared as a high-frequency shoulder to the G band resulting from the Stokes scattering by a longitudinal optical phonon. In either case, the 2D line that can be described as a single Lorentzian peak is characteristic of thin flakes comprising fewer than five graphene layers that are positioned one on top of the other in a random orientation.[19,20] This result is clearly different from the doublet 2D shape of graphite, which consists of two components $2D_1$ and $2D_2$ indicative of an unperturbed ABAB stacking sequence along the *c*-direction of the bulk material.[19,20] It was also observed that a shift of about 79 cm^{-1} to lower wavenumbers occurred for the 2D band of graphene as

dx.doi.org/10.1021/jp401736n | J. Phys. Chem. C 2013, 117, 11811−11817

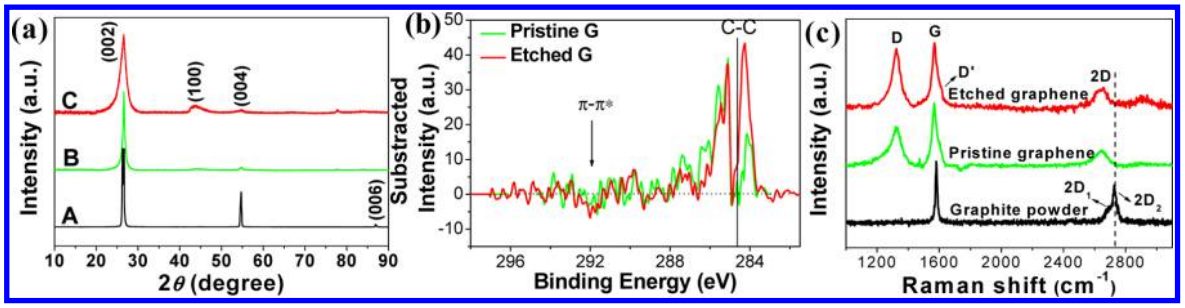

Figure 5. (a) XRD pattern of graphite (A), graphene before (B) and after (C) etching (650 °C, 0.3 mL min^{-1} H_2O vapor). (b) XPS spectra of pristine graphene and etched graphene after subtraction of the spectrum from graphite. (c) Raman modes for thin films prepared from dispersions of pristine and etched graphene in *i*-PrOH compared with bulk graphite powder for laser excitation energy E_{exc} = 1.96 eV. The spectra are normalized based on the G-mode peak intensity.

compared to graphite. The peak intensity of the D band relative to the G band (M_D/M_G) increased from 0.58 ± 0.08 to 0.95 ± 0.08, suggesting the formation of more defects during steaming. The defect population can be dominated by edge defects from small graphene flakes that were obtained due to etching effects. The in-plane crystallite size of etched graphene was determined to be approximately 24 ± 3 nm based on the integrated intensity ratio of the D and G band with a Gaussian fit (A_D/A_G) using the equation $560(A_D/A_G)^{-1}/E^4$, where E is the laser energy (1.96 eV).[13] This size is significantly lower than 36 ± 2 nm for pristine graphene. A correlation of the D/G peak intensity ratio and flake length by L (nm) ≈ $260/(\Delta M_D/M_G)$ allowed for a rough estimation of the flake length, which was reduced from 448 ± 62 to 274 ± 23 nm after etching.[21] The distance between defects, L_D, and the defect density in the basal plane of etched graphene, n_D, was calculated to be 17.51 ± 0.74 nm and 1.02 × 10^{11} ± 8.59 × 10^9 cm^{-2}, respectively, using the approximations of L_D^2 (nm^2) = $4300(M_D/M_G)^{-1}/E^4$ and n_D (cm^{-2}) = 7.3 × $10^9E^4(M_D/M_G)$.[22] In contrast to the observation that both the G and 2D modes shift significantly to higher frequency with oxidation in O_2[19] or doping in NH_3 at high temperatures,[23] no appreciable shift was found here probably due to the relatively mild nature of the etching.

A standard open-aperture Z-scan apparatus was used to measure the NLO properties of pristine and etched graphene and C_{60}. As shown in Figure 6a, all scans exhibited a reduction in transmission around the focus of the lens, indicating a typical optical limiting property. β_{eff} was deduced from the Z-scan data using a curve fitting theory based on an intensity-dependent extinction coefficient.[24] Etched graphene possesses larger β_{eff} than pristine graphene and even C_{60} irrespective of the alteration of the incident laser pulsed energy from 40 to 189 μJ. More interestingly, it was found that etched graphene exhibits much better optical limiting performance in comparison with pristine graphene and C_{60} at the same level of linear transmission (Figure 6b). In contrast to the nonlinear scattering for pristine graphene and the nonlinear absorption for C_{60}, the superior optical limiting performance of etched graphene could be attributed to the effective combination of both effects. Lateral size effects have been shown to impact the optical limiting behavior of graphene; i.e., larger graphene sheets exhibit a better limiting response.[11] However, size-related nonlinear scattering may not play a key role here, taking into account the reduction in flake size coupled with an increase in β_{eff}. It is likely that defects induced by etching may contribute to the enhancement of the optical limiting performance, which may be associated with the presence of a finite band gap in graphene after etching.[12]

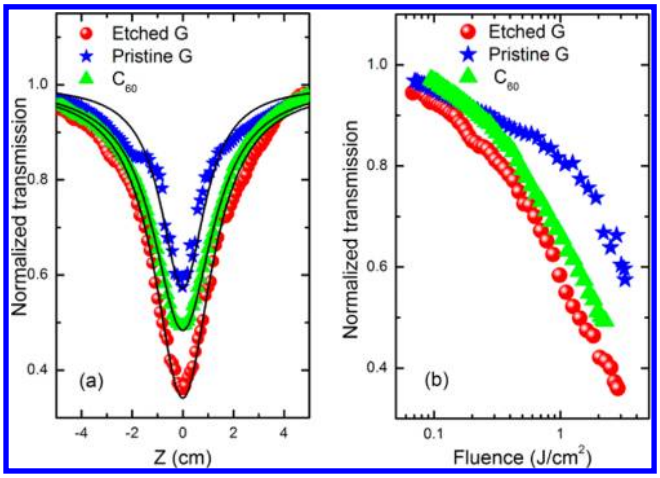

Figure 6. (a) Z-scan curves at an incident pulse energy of 120 μJ and (b) optical limiting performances of etched and pristine graphene and C_{60}.

The etching mechanism here is due to the catalytic steam gasification of carbon, where carbon species dissociate on the Fe NPs and react with dissociatively adsorbed H_2O at the NP surfaces (Figure S6, Supporting Information). The etching role of water vapor was confirmed by TEM observations that no detectable etching occurred in the absence of water. This also rules out the possibility of catalytic hydrogenation of graphene in this work. On the other hand, almost no etching effect was observed for pristine graphene without the catalytic NPs under otherwise identical conditions (Table 1 and Supporting Information Figure S7). This occurrence is a strong indication of the catalytic function of the NPs in the process. As is the case for oxidation in air, steam etching should also start from the

Table 1. Carbon Atoms (mmol) Etched off As a Function of the Experimental Conditions

sample	T (°C)	steam flow ($mL\ min^{-1}$)	Fe mass loading content (%)	C consumed (mmol)
pristine G	650	0.3	0	0.00282
Fe–G	550	0.3	3	0.00294
Fe–G	650	0.3	3	0.0342
Fe–G	750	0.3	3	0.0937
Fe–G	650	0.075	3	0.0106
Fe–G	650	0.3	1.5	0.0102
Fe–G	650	0.3	6	0.0570

dx.doi.org/10.1021/jp401736n | J. Phys. Chem. C 2013, 117, 11811−11817

relatively more reactive sp^3 carbon sites distributed mostly at the graphene edges.

The etching process can be readily tuned by controlling the reaction temperature, steam concentration, and the loading density of the NPs (Table 1). Integrating the amount of produced CO over the time of reaction allows us to quantify the etching level of graphene, which has rarely been realized in previous work. A steady increase in the quantities of carbon atoms consumed (m_G) was found with the rise in reaction temperature from 550 to 750 °C. The etching effect became very low at T = 550 °C indicating that the etching temperature must exceed a certain threshold. Increasing the water vapor concentration from 0.075 to 0.3 mL min^{-1} resulted in an enhancement of m_G by ~3.2%. Alternatively, a larger m_G was obtained at higher loading content of the catalytic NPs on graphene. We note that the etching degree of graphene is rather small, when the loading content is below 1.5 wt %. At high loading levels (>3 wt %), the enhancement of m_G is less strong.

CONCLUSION

Nanostructured few-layer graphene was fabricated through the etching of graphene via catalytic steam gasification of carbon by Fe NPs. The etching occurs selectively at the interface between graphene and the Fe NPs and can be easily controlled by the reaction temperature, the steam concentration, as well as the loading of the catalytically active NPs. Nanostructured graphene exhibits superior optical limiting performances compared to both pristine graphene and C_{60} showing a large potential in nanophotonic devices.

ASSOCIATED CONTENT

Supporting Information

TEM, SEM, EDX, UV, XPS, and Raman analyses, schematic illustration of the etching process, and the rate of formation of CO over reaction time at varying conditions. This material is available free of charge via the Internet at http://pubs.acs.org.

AUTHOR INFORMATION

Corresponding Author

*E-mail: muhler@techem.rub.de; jwang@siom.ac.cn.

Notes

The authors declare no competing financial interest.

ACKNOWLEDGMENTS

Zhenyu Sun thanks the Alexander von Humboldt Foundation for an experienced researcher fellowship. This work was supported in part by the 100-Talent Program of Chinese Academy of Sciences, the National Natural Science Foundation of China (No. 61178007), and Science and Technology Commission of Shanghai Municipality (STCSM Nano Project No. 11 nm0502400, Pujiang Talent Program 12PJ1409400).

REFERENCES

(1) Compton, O. C.; Nguyen, S. T. Graphene Oxide, Highly Reduced Graphene Oxide, and Graphene: Versatile Building Blocks for Carbon-Based Materials. *Small* **2010**, *6*, 711−723.

(2) Son, Y. W.; Cohen, M. L.; Louie, S. G. Half-Metallic Graphene Nanoribbons. *Nature* **2006**, *444*, 347−349.

(3) Xie, L. M.; Jiao, L. Y.; Dai, H. J. Selective Etching of Graphene Edges by Hydrogen Plasma. *J. Am. Chem. Soc.* **2010**, *132*, 14751−14753.

(4) Han, M. Y.; Ozyilmaz, B.; Zhang, Y. B.; Kim, P. Energy Band-Gap Engineering of Graphene Nanoribbons. *Phys. Rev. Lett.* **2007**, *98*, 206805.

(5) Tapaszto, L.; Dobrik, G.; Lambin, P.; Biro, L. P. Tailoring the Atomic Structure of Graphene Nanoribbons by Scanning Tunnelling Microscope Lithography. *Nat. Nanotechnol.* **2008**, *3*, 397−401.

(6) Masubuchi, S.; Ono, M.; Yoshida, K.; Hirakawa, K.; Machida, T. Fabrication of Graphene Nanoribbon by Local Anodic Oxidation Lithography Using Atomic Force Microscope. *Appl. Phys. Lett.* **2009**, *94*, 082107.

(7) Lim, G. K; Chen, Z. L.; Clark, J.; Goh, R. G. S.; Ng, W. H.; Tan, H. W.; Friend, R. H.; Ho, P. K. H.; Chua, L. L. Giant Broadband Nonlinear Optical Absorption Response in Dispersed Graphene Single Sheets. *Nat. Photonics* **2011**, *5*, 554−560.

(8) Wang, J.; Hernandez, Y.; Lotya, M.; Coleman, J. N.; Blau, W. J. Broadband Nonlinear Optical Response of Graphene Dispersions. *Adv. Mater.* **2009**, *21*, 2430−2435.

(9) Feng, M.; Zhan, H. B.; Chen, Y. Nonlinear Optical and Optical Limiting Properties of Graphene Families. *Appl. Phys. Lett.* **2010**, *96*, 033107.

(10) Feng, M.; Sun, R. Q.; Zhan, H. B.; Chen, Y. Lossless Synthesis of Graphene Nanosheets Decorated with Tiny Cadmium Sulfide Quantum Dots with Excellent Nonlinear Optical Properties. *Nanotechnology* **2010**, *21*, 075601.

(11) Zhao, B. S.; Cao, B. B.; Zhou, W. L.; Li, D.; Zhao, W. Nonlinear Optical Transmission on Nanographene and Its Composites. *J. Phys. Chem. C* **2010**, *114*, 12517−12523.

(12) Zhou, Y.; Bao, Q. L.; Tang, L. A. L.; Zhong, Y. L.; Loh, K. P. Hydrothermal Dehydration for the "Green" Reduction of Exfoliated Graphene Oxide to Graphene and Demonstration of Tunable Optical Limiting Properties. *Chem. Mater.* **2009**, *21*, 2950−2956.

(13) Sun, Z. Y.; Masa, J.; Liu, Z. M.; Schuhmann, W.; Muhler, M. Highly Concentrated Aqueous Dispersions of Graphene Exfoliated by Sodium Taurodeoxycholate: Dispersion Behavior and Potential Application as a Catalyst Support for the Oxygen-Reduction Reaction. *Chem.—Eur. J.* **2012**, *18*, 6972−6978.

(14) Xia, W.; Hagen, V.; Kundu, S.; Wang, Y. M.; Somsen, C.; Eggeler, G.; Sun, G. G.; Grundmeier, G.; Stratmann, M.; Muhler, M. Controlled Etching of Carbon Nanotubes by Iron-Catalyzed Steam Gasification. *Adv. Mater.* **2007**, *19*, 3648−3652.

(15) Yin, Y. D.; Rioux, R. M.; Erdonmez, C. K.; Hughes, S.; Somorjai, G. A.; Alivisatos, A. P. Formation of Hollow Nanocrystals through the Nanoscale Kirkendall Effect. *Science* **2004**, *304*, 711−714.

(16) Liu, L.; Ryu, S. M.; Tomasik, M. R.; Stolyarova, E.; Jung, N.; Hybertsen, M. S.; Steigerwald, M. L.; Brus, L. E.; Flynn, G. W. Graphene Oxidation: Thickness-Dependent Etching and Strong Chemical Doping. *Nano Lett.* **2008**, *8*, 1965−1970.

(17) Campos, L. C.; Manfrinato, V. R.; Sanchez-Yamagishi, J. D.; Kong, J.; Jarillo-Herrero, P. Anisotropic Etching and Nanoribbon Formation in Single-Layer Graphene. *Nano Lett.* **2009**, *9*, 2600−2604.

(18) Shih, C. J.; Vijayaraghavan, A.; Krishnan, R.; Sharma, R.; Han, J. H.; Ham, M. H.; Jin, Z.; Lin, S. C.; Paulus, G. L. C.; Reuel, N. F.; Wang, Q. H.; Blankschtein, D.; Strano, M. S. Bi- and Trilayer Graphene Solutions. *Nat. Nanotechnol.* **2011**, *6*, 439−445.

(19) Ferrari, A. C.; Meyer, J. C.; Scardaci, V.; Casiraghi, C.; Lazzeri, M.; Mauri, F.; Piscanec, S.; Jiang, D.; Novoselov, K. S.; Roth, S.; Geim, A. K. Raman Spectrum of Graphene and Graphene Layers. *Phys. Rev. Lett.* **2006**, *97*, 187401.

(20) Ferrari, A. C. Raman Spectroscopy of Graphene and Graphite: Disorder, Electron-Phonon Coupling, Doping and Nonadiabatic Effects. *Solid State Commun.* **2007**, *143*, 47−57.

(21) O'Neill, A.; Khan, U.; Nirmalraj, P. N.; Boland, J.; Coleman, J. N. Graphene Dispersion and Exfoliation in Low Boiling Point Solvents. *J. Phys. Chem. C* **2011**, *115*, 5422−5428.

(22) Tomai, T.; Kawaguchi, Y.; Honma, I. Nanographene Production from Platelet Carbon Nanofiber by Supercritical Fluid Exfoliation. *Appl. Phys. Lett.* **2012**, *100*, 233110.

(23) Guo, B. D.; Liu, Q. A.; Chen, E. D.; Zhu, H. W.; Fang, L. A.; Gong, J. R. Controllable N-Doping of Graphene. *Nano Lett.* **2010**, *10*, 4975−4980.
(24) Sheik-Bahae, M.; Said, A. A.; Wei, T. H.; Hagan, D. J.; Van Stryland, E. W. Sensitive Measurement of Optical Nonlinearities using a Single Beam. *IEEE J. Quantum Electron.* **1990**, *QE-26*, 760−769.